



Effects of horizontal resolution and air-sea coupling on simulated moisture sources for regional East Asian precipitation

Liang Guo¹, Ruud J. van der Ent², Nicholas P. Klingaman¹, Marie-Estelle Demory³, Pier Luigi Vidale¹, Andrew G. Turner^{1,4}, Claudia C. Stephan⁵, and Amulya Chevuturi¹

¹National Centre for Atmospheric Science, Department of Meteorology, University of Reading, United Kingdom

²Department of Water Management, Faculty of Civil Engineering and Geosciences, Delft University of Technology, Delft, the Netherlands

³Department of Environmental Systems Science, Institute for Atmospheric and Climate Science, ETH Zürich, Zürich, Switzerland

⁴Department of Meteorology, University of Reading, Reading, United Kingdom

⁵Max Planck Institute for Meteorology, Hamburg, Germany

Correspondence: Liang Guo (l.guo@reading.ac.uk)

Abstract. Precipitation over East Asia (EA) simulated in six experiments using the Met Office Unified Model (MetUM) is compared with observations and ERA-Interim reanalysis. These simulations are performed at resolutions of 200 - 40 km and with both atmosphere-only and air-sea coupled configurations. EA precipitation in MetUM is systematically overestimated, especially over southeastern EA and the Tibetan Plateau. Moisture sources for simulated and observed regional EA precipitation are traced using the Water Accounting Model-2layers (WAM-2layers) - a moisture tracking model that traces moisture sources using a combination of evaporation, atmospheric moisture and circulation. Biases in moisture sources are linked to biases in precipitation. For southeastern EA, positive precipitation biases are linked to errors in mid-latitude sources rather than tropical ocean sources. Increasing resolution reduces precipitation biases over the Tibetan Plateau. From the perspective of moisture source, this reduction comes from reduced remote moisture source that is blocked by the better representations of topography at higher resolution. Including coupling does not necessarily improve EA precipitation, however, coupling alters moisture sources. Because the effect of coupling on moisture source varies on location and sign, the collective impact on EA precipitation may not be noticeable. By using WAM-2layers, these changes in moisture sources can be attributed to changes in SST, circulation and associated evaporation. WAM-2layers can be a useful tool to identify model biases that cause biases in regional precipitation.

15

1 Introduction

Identifying moisture sources for East Asian (EA) precipitation has long been a challenge that motivates the scientific community. Understanding EA precipitation and its variability also has socio-economical values in the areas such as the water resource



management, agricultural irrigation and hydroelectric power generation. Different methods have been applied to identify moisture sources for EA precipitation, from diagnosing the net moisture flux on boundaries of a studied region (e.g., Zhou and Yu, 2005), to using simple analytic models (e.g., Guo et al., 2018), to tracking moisture using the atmospheric moisture conservation equation under either Lagrangian or Eulerian frameworks (e.g., Wei et al., 2012; Zhang et al., 2017; Guo et al., 2019; Fremme and Sodemann, 2019).

The understanding of moisture sources for EA precipitation has been changing in recent years. As EA is influenced by the EA summer monsoon (EASM), early studies considered the adjacent oceans (both the Pacific and Indian Oceans) as the major direct (i.e., without being precipitated and re-evaporated) moisture source for EA precipitation and its interannual variability (Zhou and Yu, 2005; Wang and Chen, 2012). However, with recent advantages in moisture tracking models, moisture sources could be identified more accurately, as these models implemented the atmospheric moisture conservation equations at higher temporal and spatial resolutions. As a result, land surface contributions were recognised (Wei et al., 2012; Zhang et al., 2017; Fremme and Sodemann, 2019) and replaced oceans as the major source for EA precipitation, especially over inland and mid-latitude regions. On the other hand, due to frozen soil and snow cover over the Eurasian continent during boreal winter, moisture contributions from land surfaces reduced but contributions from water bodies to the west of EA (i.e., from the Mediterranean Sea and the northern Atlantic Ocean) increased, as this moisture can be transported along the mid-latitude westerlies (Guo et al., 2019).

Correctly simulating precipitation and the hydrological cycle in contemporary Global Climate Models (GCMs) remains challenging (Liepert and Previdi, 2012). These challenges are also manifested at regional scales. Model biases in precipitation and the hydrological cycle over EA have been reported and analysed in previous studies (Wen et al., 2016; Yang et al., 2014; Ou et al., 2013; Chen and Sun, 2015; Jiang et al., 2015). Uncertainties notwithstanding, improvements on simulating precipitation and the hydrological cycle have been made with increased horizontal resolution and including air-sea coupling. By investigating eighteen GCMs with horizontal resolution varying between 100 km and 20 km, Vannière et al. (2018) found improved precipitation over land globally with the increase in horizontal resolution. They also found improved precipitation patterns and amplitudes at regional scale, due to more realistic seasonal circulation with increased horizontal resolution. Similar improvements in the global hydrological cycle with increased horizontal resolution have also been reported in Terai et al. (2018) and Demory et al. (2014). Improvements at regional scales due to increased horizontal resolution have been reported over South Asia (Johnson et al., 2016; Ogata et al., 2017), Maritime Continent (Schiemann et al., 2014), tropical Africa (Vellinga et al., 2016) and for the mid-latitude storm track (van Haren et al., 2015). Over EA, Stephan et al. (2018b) found that the seasonal mean precipitation and its interannual variability are improved with increased resolution in the Met Office Unified Model, particularly near orography in southwest China (although the improvement is small relative to the model mean biases).

The oceans play an important role in the global hydrological cycle, as about 85% of the evaporation and 77% of the precipitation occur over the ocean (Schanze et al., 2010). Air-sea coupling makes the air-sea fluxes in GCMs more realistic, in terms of both heat and water, and therefore changes water/precipitation distributions in models (Ratnam et al., 2015; Dong et al., 2017; Hirons et al., 2018). Over EA, previous studies have shown that simulated precipitation has been improved due to both local and remote air-sea interactions (e.g., Fu et al., 2002). Although, introducing air-sea coupling can also introduce sea surface



temperature (SST) biases (Gupta et al., 2013), Yang et al. (2019) suggested that coupled models represent EA precipitation
55 more realistically due to compensating errors from SST biases that originate from atmosphere models.

Although simulated EA precipitation has improved with resolution and coupling, biases remain prominent and their causes
are still unclear (Sperber et al., 2013). Therefore, in this study, systematic biases of EA precipitation in a set of numerical
experiments are investigated from the perspective of moisture sources, which are identified using a moisture tracking model.
Biases in precipitation are linked to biases in moisture source both remotely and locally, and be further attributed to biases in
60 evaporation, circulation and atmospheric moisture. Impacts of resolution and coupling on simulated EA precipitation will also
be investigated from the perspective of moisture sources. The set of numerical experiments has been conducted using the Met
Office Unified Model (MetUM) Global Atmosphere 6.0 (GA6) and Global Coupled configuration 2.0 (GC2) at three horizontal
resolutions. The moisture tracking model is the Water Accounting Model (WAM-2layers). WAM-2layers has been applied to
EA precipitation in previous studies (Keys et al., 2014; Guo et al., 2019) with different reanalysis datasets. Compared to other
65 tracking methods, its efficiency makes it a more suitable tool to work with high-resolution and long-term climate simulations.

More details about MetUM and WAM-2layers are given in Section 2. Simulated EA precipitation and moisture sources are
compared to observations and reanalyses in Section 3. Differences in moisture sources for EA precipitation due to resolution
and coupling are discussed in Section 4. Discussion and conclusions are in Section 5.

2 Data and Methods

70 2.1 Data

The European Centre for Medium-Range Weather Forecasts Interim reanalysis data set (ERA-Interim; Berrisford et al., 2011;
Dee et al., 2011) from 1979-2016 is used to validate simulated precipitation and to drive WAM-2layers. Daily mean variables
on a single level (precipitation, evaporation, surface pressure and near-surface specific humidity) and model levels (horizontal
wind and specific humidity) are used.

75 Observational daily precipitation over EA is obtained from the Asian Precipitation-Highly-Resolved Observational Data
Integration Towards Evaluation (APHRODITE; Yatagai et al., 2012) dataset. APHRODITE utilises rain-gauge data with pro-
cesses of quality control and is available from 1951-2007. To match with the ERA-Interim and MetUM simulations, data from
1979 onward are used.

SST is evaluated against the Operational Sea Surface Temperature and Sea Ice Analysis (OSTIA Donlon et al., 2012). As
80 coupled simulations are configured to represent present day climate, OSTIA data from 1979 to 2016 is used.

2.2 Met Office Unified Model and experiments

The MetUM Global Atmosphere 6.0 (GA6; Walters et al., 2017) and Global Coupled 2.0 configuration (GC2; Williams et al.,
2015) are used. GA6 includes a relatively new dynamical core, which significantly increases mid-latitude variability and
increases variability in the tropics. GC2 couples GA6 with with an ocean model (Nucleus for European Modelling of the



85 Ocean (NEMO); Madec, 2008) and a sea-ice model (the Community Ice CodE and the Los Alamos Sea Ice Model (CICE); Hunke and Lipscomb, 2004) via the coupler OASIS3 (Valcke, 2013) of 3 hourly frequency. GC2 showed an improvement over previous configurations, particularly in terms of modes of variability, e.g., mid-latitude and tropical cyclone intensities, the Madden-Julian Oscillation and El Niño Southern Oscillation (Williams et al., 2015).

Six MetUM simulations are used, which can be grouped into three pairs. Each pair includes an atmosphere-only simulation (A) and a coupled simulation (C), which have the same atmospheric resolution. Three resolutions are used, 192 longitude points × 145 latitude points (N96), 432 × 325 (N216) and 1024 × 769 (N512). Therefore, six simulations used here are denoted as AN96, CN96, AN216, CN216, AN512 and CN512. The equivalent atmospheric grid spacing in longitude at the equator is 200km, 90km and 40km, respectively. The atmosphere model has 85 hybrid height levels in the vertical covering 0-85km. The ocean model uses 75 vertical levels and the ORCA025 tri-polar grid which has 0.25° resolution at the equator. Periods of simulation are listed in Table 1. Simulations match the period of ERA-Interim, except for the N512 simulations, which have a shorter simulation period.

2.3 Water Accounting Model-2layers

WAM-2layers is a moisture tracking model developed by van der Ent et al. (2013, 2014). WAM-2layers is based on the atmospheric water conservation equation and combines information from precipitation, evaporation, atmospheric circulation and moisture to determine sources or sinks of moisture originating from a specified region. In this study, WAM-2layers is applied to backward trace moisture sources for regional precipitation over EA in both ERA-Interim reanalysis and MetUM simulations. Daily precipitation in the target EA region is fed into WAM-2layers, which is integrated backward using circulation and humidity data on model/pressure levels. The domain and magnitude of the moisture source are calculated using the point of last evaporation for precipitation falling in the target region. A detailed description about WAM-2layers and its setup over EA is given in Guo et al. (2019). As EA crosses several climatic zones and has inhomogeneous hydrological features, EA is first divided into five subregions according precipitation minus evaporation and topography (Figure 1). These regions are southeastern EA (region 1), Tibetan Plateau (region 2), central-eastern EA (region 3), northwestern EA (region 4) and northeastern EA (region 5). A similar division has been used in Guo et al. (2018), where detailed discussion about the division is given.

3 Differences to observation/reanalysis

3.1 Precipitation

Figure 2 shows annual mean EA precipitation in APHRODITE, MetUM AN96 and ERA-Interim, and biases of AN96 and ERA-Interim against APHRODITE. AN96 (Figure 2b) captures the major features of precipitation over EA, i.e., the south-north precipitation gradient, the precipitation maxima over the Sichuan Basin and southeastern China. However, compared to APHRODITE (Figure 2c), AN96 overestimates precipitation over the Tibetan Plateau, the Sichuan Basin and southeastern China, but underestimates precipitation over the southern slope of the Himalayas. There are also biases over southern Asia, i.e.,



the Indian Peninsula, Bangladesh and the Indochina Peninsula. These biases are also common in other MetUM simulations and have been reported in previous studies (e.g., Stephan et al., 2018a). Comparing ERA-Interim to APHRODITE, Figure 2e shows that ERA-Interim overestimates precipitation over southwestern China and the Tibetan Plateau. These biases in ERA-Interim will affect the accuracy of the moisture source calculations over these regions. However, using ERA-Interim precipitation remains as only option because it is physically consistent with other ERA-Interim variables, i.e., wind, humidity and evaporation, therefore offers a reasonably closed water budget for WAM-2layers.

These biases are also reflected in seasonal and regional means over EA subregions (Figure 3). Both ERA-Interim and MetUM simulations overestimate precipitation over southeastern EA (region 1), with biases in MetUM being larger. Precipitation over the Tibetan Plateau (region 2) is also overestimated in ERA-Interim and MetUM. With increased resolution, biases in simulations reduce, especially with comparing from low (N96) to medium resolution (N216). A detailed analysis of the resolution-related changes in moisture sources is discussed in Section 4.1. Biases over regions 3 and 4 are smaller in coupled simulations compared to atmosphere-only simulations, especially in JJA and in medium and high-resolution simulations. This difference is due to a weak western North Pacific subtropical high (WNPSH) is in the coupled simulations (not shown). The weak WNPSH reduces moisture transport from low latitudes (region 1) to mid latitudes (regions 3 and 4), which therefore reduces the positive biases (Figure 4f, h). This weak WNPSH has also been identified in previous studies (e.g., Rodríguez et al., 2017). To further investigate these biases, moisture sources of simulated EA precipitation are traced and compared to ERA-Interim.

3.2 Moisture source

Figure 4 shows the annual mean moisture sources and the vertically integrated moisture fluxes for five EA subregions using ERA-Interim. The differences between AN96 and ERA-Interim are also shown in Figure 4. Compared to ERA-Interim, AN96 transports less moisture from low latitudes but more from middle latitudes for all EA subregions. These differences are largely associated with differences in moisture fluxes (Figure 4b, d, f, h and j). In AN96, the cross-equatorial flow along the Somali Jet is too weak, but the mid-latitude westerlies is too strong. The moisture flux over region 1 is too zonal, which is consistent with a weak WNPSH, illustrated as a cyclonic moisture flux anomaly shown on Figure 4b. These differences cause less moisture to be transported from low latitude to middle latitude and reduced moisture contribution from southern China to regions 3, 4 and 5 in AN96 (Figure 4f, h and j). Over the Tibetan Plateau, AN96 transports less moisture than ERA-Interim over the whole source domain, except eastern Tibet. This indicates that the simulated precipitation over the Tibetan Plateau in AN96 relies more on local sources but less on remote sources.

The contribution of local moisture to precipitation is measured using the precipitation recycling ratio, defined as the proportion of precipitation in the target region that is contributed by the evaporation over the same region. Figure 5 shows the annual cycle of the precipitation recycling ratio for five EA subregions. The simulations can reproduce the annual cycles over regions 1, 3 and 4 (Table 2), but overestimate the recycling ratio over regions 2 (summer and autumn) and 5 (spring and autumn).

The simulated and ERA-Interim remote moisture sources are compared using its shape. To assist comparison, instead of showing maps of seasonal moisture source, the mass centres of the moisture sources from the simulations and ERA-Interim are compared collectively in Figure 6. Figure 6 shows the mass centres for all five regions in DJF and JJA. The mass centres



150 are measured using the moisture source regions that account for 80% of precipitation in the target regions, similar to those in Figure 4. The mass centres were also measured using threshold at 50% and 65% of precipitation; the results are consistent and not sensitive to the choice of threshold. As shown in Figure 6, the simulated mass centres show consistent seasonal variations as in ERA-Interim. However, there are systematic differences between the simulations and ERA-Interim, as well as among the simulations.

155 Over region 1 in JJA (coloured triangles in Figure 6a), the mass centres of simulated moisture sources are located approximately 5° north of the ERA-Interim mass centre. This difference is due to the weak cross-equatorial moisture transport from the tropical Indian Ocean in all simulations, as shown in Figure 7e, which leads to an underestimation of the moisture contributions from low latitudes. It indicates that the wet biases in JJA over region 1 in the simulations (Figure 3) are not necessarily linked to excessive oceanic evaporation as one might naively think. In DJF (coloured circles in Figure 6a), however, the mass centres
160 of the simulated moisture sources are located 10° west of the ERA-Interim mass centre. Similar shifts are shown for regions 2 and 3 (Figure 6b, c). Compared to regions 1, 2 and 3 in JJA, the northward shift of the mass centres for regions 4 and 5 is smaller (coloured triangles in Figure 6d, e). This is because regions 4 and 5 are situated over the mid-latitudes, therefore, the tropical impacts associated with the EASM are less. In DJF over regions 4 and 5 (coloured circles in Figure 6d, e), simulated
165 mass centres are located east of the ERA-Interim mass centre, especially, for high-resolution simulations, CN216, AN512 and CN512, wherein the eastward shift can be as large as 30° . To explain this difference, moisture sources for region 5 in DJF from CN512 are compared to ERA-Interim (Figure 7f). In CN512, too much moisture originates from regions east of region 5, i.e., from the Seas of Japan and Okhotsk, but too little from regions west of region 5, especially, from the Mediterranean Sea, the Red Sea and the Persian Gulf. This eastward shift is smaller in low-resolution simulations (AN96, CN96 and AN216). More details are discussed in Section 4.3.

170 The remote moisture sources are further divided into four sections (tropical sea, tropical land, extra-tropical sea and extra-tropical land). Together with the local source (measured as the precipitation recycling ratio), the contributions from these sections are compared in Table 3. For the annual mean contribution, the simulations can reproduce the primary sources identified from ERA-Interim for all EA subregions, i.e., tropical sea for region 1 and extra-tropical land for regions 2, 3, 4 and 5. On the other hand, for seasonal mean contributions, discrepancies between the simulations and ERA-Interim are large. Even
175 the primary sources are different between the simulations and ERA-Interim (as boldface values highlighted in Table 3). Since these discrepancies are also sensitive to resolution and coupling, more details are discussed in Section 4.3.

4 Differences in moisture source due to model resolution and coupling

Comparisons in the previous section show that MetUM simulations have systematic biases against ERA-Interim in both precipitation and moisture sources. Despite increasing resolution and including coupling, these systematic biases between MetUM
180 simulations and ERA-Interim remain. However, there is evidence to show that precipitation and moisture sources are sensitive to resolution and coupling. Therefore, these changes in moisture source are discussed here; links between changes in moisture source and precipitation are also made in the section.



4.1 Change with resolution

As shown in Figure 3b, over the Tibetan Plateau, the simulations have smaller precipitation biases against APHRODITE than
185 ERA-Interim, especially in MAM and JJA. From the perspective of moisture source (Figure 4d), this improvement is attributed
to the reduced remote contribution. Also shown in Figure 3b, increasing resolution reduces the mean precipitation bias over the
Tibetan Plateau. Similar results have also been found in previous studies (e.g., Curio et al., 2015), which showed that higher
resolution improves the representation of topography in models; steeper topography blocks remote moisture transport. On the
other hand, the local moisture contribution is enhanced with resolution (Figure 5b) because the steeper topography reduces the
190 outflow of local moisture. In MetUM simulations, the enhanced local moisture source is located over eastern Tibet (Figure 8a,
b and c). This is partly because eastern Tibet is wetter than western Tibet, partly because the north-south orientated valleys
over southeast Tibet are the major pathway for remote moisture. By reducing the remote contribution, the local contribution
becomes larger. This is demonstrated (Figure 8d) by the opposing trends in the tracked local evaporation over eastern Tibet
(increase) and the low-level wind along its southern boundary (decrease).

195 4.2 Change with coupling

To investigate impacts of coupling on moisture sources, we focus on region 1, where the oceans are the major contributors
(according to Table 3). Differences in moisture source over region 1 in JJA between coupled and atmosphere-only simulations
in different resolutions are shown in Figure 9. Regardless of resolution, coupled simulations always show consistent differences
against atmosphere-only simulations, which include a reduced moisture contribution from the Indian Ocean but an increased
200 moisture contribution from the Pacific Ocean. The reduced moisture contribution over the Indian Ocean is linked to the cold
SST bias over the Arabian Sea, as demonstrated in Figure 9d. This cold SST bias reduces local evaporation, which reduces
its contribution to precipitation over region 1. This cold SST bias has also been reported in previous studies with MetUM
(e.g., Marathayil et al., 2013). On the other hand, there is not a consistent SST bias associated with the increased moisture
contribution over the Pacific Ocean (Figure 9d). Instead, there is a consistent increase in the low-level wind in all coupled
205 simulations (Figure 9d). As mentioned in Section 3, this wind bias is due to the EASM flow being too zonal in all coupled
simulations. The positive low-level wind bias over the South China Sea intensifies local evaporation. Associated with this
wind bias is a weak WNPSH, which is demonstrated in Figure 9a, b and c as the cyclonic anomaly over the southeast coast
of EA. This cyclonic anomaly converges the enhanced evaporation over the same location and transports more moisture from
the South China Sea into region 1. As these two changes in moisture sources due to coupling show opposite signs and similar
210 magnitudes, when attributing them collectively to changes in precipitation, the differences of precipitation over region 1 in JJA
between atmosphere-only and coupled simulations are small (Figure 3a). However, it does not necessarily mean that changes
in SST, evaporation or circulation are also small.



4.3 Shift of the major moisture source over mid-latitude regions

In Section 3.2, it has been mentioned that simulated mass centres for regions 4 and 5 shift eastward compared to ERA-Interim and the shift is sensitive to resolution (Figure 6d, e). A similar division regarding resolution is shown in Table 3 as identifying major moisture contributors to seasonal mean precipitation. In Table 3, moisture contribution from different remote sections (tropical sea, tropical land, extra-tropical sea and extra-tropical land) and local source are estimated. On annual scales, the major moisture source for region 1 is tropical sea, but it is extratropical land for other regions. The results are consistent between simulations and ERA-Interim. On seasonal scales, however, major sources identified from simulations and ERA-Interim are inconsistent for regions 4 and 5 in DJF. For regions 4 and 5 in DJF, the major moisture source shifts from extratropical land to extratropical sea in ERA-Interim (boldface values in Table 3). This shift is partly due to the reduced evapotranspiration over the frozen Eurasian land surface, and partly due to the enhanced moisture transport along the intensified winter mid-latitude westerly jet that transports moisture from the Mediterranean Sea, the Black Sea and the Caspian Sea (Guo et al., 2019). As shown in Table 3, this shift from land to sea is captured by simulations with higher resolutions, CN216, AN512 and CN512. However, there is no evidence for improvements in mean precipitation over regions 4 and 5 in DJF (Figure 3d and e). On the contrary, maps of moisture source over region 5 in DJF show that all simulations are systematically different from ERA-Interim (Figure 10). Simulations receive less moisture from sources west of region 5 but more from sources east of region 5, which explains the eastward shift of the mass centre in all simulations. The larger eastward shift in simulations with higher resolutions is due to the stronger positive source biases over the Seas of Japan and Okhotsk.

Since this bias originates from the ocean, SST biases between simulations and observation are shown in Figure 11 for different resolutions. With increase in resolution to N216 and N512, the positive SST bias over the Sea of Japan increases, and the sign of SST bias over the Sea of Okhotsk switches from negative to positive. These positive SST biases in higher resolution simulations increase biases in local evaporation, which causes the positive moisture source biases over these regions in higher resolution.

SST biases explain the eastward shift of mass centres in higher resolution coupled simulations, such as CN216 and CN512. However, it cannot explain the shift in AN512 where there is no SST bias involved. Note that there is a similar but weaker moisture source change over the Seas of Japan and Okhotsk in all atmosphere-only simulations; this positive source change increases with resolution. Considering that precipitation over region 5 in DJF is small ($0.2 \text{ mm} \cdot \text{day}^{-1}$ as shown in Figure 3e), this positive source change with resolution eventually shifts the major moisture source in AN512.

5 Discussion and conclusion

5.1 Discussion

We use ERA-Interim as a benchmark to compare moisture sources traced from simulations. As shown in Figures 2 and 3, ERA-Interim precipitation has its own bias compared to APHRODITE. We choose to trace ERA-Interim precipitation over observed precipitation because it is physically consistent with other ERA-Interim variables used in WAM-2layers. Therefore, the water



245 budget can be reasonably closed. Besides, ERA-Interim precipitation over EA shows the highest fidelity among reanalyses in terms of reproducing the mean and interannual variability of EA precipitation (Lin et al., 2014; Su et al., 2015).

The length of simulations for N512 is shorter than other simulations (Table 1). This may cause inconsistency when comparing results from different resolutions. Only one ensemble member per simulation is used in this study. Therefore, the robustness of the results will need further test when more ensemble members are available.

250 5.2 Conclusions

In this study, moisture sources of EA precipitation simulated by MetUM are traced using WAM-2layers and compared to ERA-Interim. The purposes of this study are: first, to link systematic biases in simulated EA precipitation to biases in moisture sources; second, to investigate sensitivities of moisture sources to model atmospheric horizontal resolution and air-sea coupling. Six MetUM simulations are used, AN96, CN96, AN216, CN216, AN512 and CN512, which denote atmosphere-only (A) and
255 air-sea coupled (C) simulations at three resolutions.

MetUM simulations can reasonably capture patterns of EA precipitation but show systematic biases against observation regardless of resolutions or coupling. These biases include overestimations over southeastern China and the Tibetan Plateau and underestimations over the southern slope of the Himalayas. Simulated precipitation is sensitive to both resolution and coupling. However, systematic errors in precipitation between simulations and observations cannot be eliminated with either
260 resolution or coupling.

Moisture sources traced from simulations agree with those from ERA-Interim in terms of the seasonal cycles of local moisture contribution and mass centres. However, systematic differences in moisture sources between simulations and ERA-Interim are noticeable. Simulated precipitation over southeastern EA (region 1) have smaller contributions from tropical oceans but more from mid-latitude sources, which is due to a weak cross-equatorial moisture flux over the Indian Ocean. For the same
265 reason, all simulated mass centres of region 1 are situated north of the mass centre in ERA-Interim, especially in JJA. Although the mean precipitation biases are small for mid-latitude EA regions (regions 4 and 5), simulated mass centres, however, are situated east of the mass centre in ERA-Interim, especially in DJF. This is because moisture in simulations originates from the Pacific Ocean for precipitation over mid-latitude EA, while it mainly originates from the Mediterranean Sea and the Atlantic Ocean in ERA-Interim. Simulated precipitation over the Tibetan Plateau has smaller biases compared to ERA-Interim, which
270 is manifested as a reduced remote contribution but an enhanced local contribution in moisture sources.

Although increasing resolution can not eliminate systematic errors in precipitation between MetUM simulations and ERA-Interim, improvements are noticeable, especially over the Tibetan Plateau. Better representation of topography at higher resolutions reduce remote moisture contribution and enhance local moisture contribution. This change is more noticeable over the eastern Tibetan Plateau, where the surface is wetter and the remote moisture can enter its southern boundary along the
275 north-south orientated valleys.

EA precipitation is not necessarily improved with coupling. However, the moisture sources associated with EA precipitations can still be changed. For example, although differences in precipitation with coupling over region 1 in JJA are small, a negative moisture source change over the Arabian Sea and a positive change over the South China Sea are found in all cou-



280 pled simulations. These changes are associated with changes in SST and circulation that are introduced by including air-sea
coupling. These changes in moisture sources have different signs, therefore, the collective impact on precipitation over a target
region cannot necessarily be detected through analysis of mean precipitation alone. However, this study shows the usefulness
of WAM-2layers in identifying model biases in a range of variables that relate to precipitation, and evaluating the sensitivity
of those biases to changes in model resolution or physics.

285 Simulations at higher resolutions capture a seasonal shift of the major moisture contributor over regions 4 and 5 in DJF,
in which the major contributor shifts from mid-latitude land to mid-latitude ocean. In reanalysis, this shift is caused by a
reduced land surface evapotranspiration and an enhanced moisture transport via mid-latitude westerlies from oceans west of
the target regions. However, none of the simulations can reproduce this mechanism. Instead, shifts in simulations are caused
by an increasing moisture source over the Pacific, which is related to the increase in resolution.

290 In summary, we have shown in this study that, to better understand precipitation biases in simulations, it is necessary to go
a step further by connecting precipitation biases to biases in other related variables using a moisture tracking tool that is built
upon the atmospheric moisture conservation equation. We have also shown that the WAM-2layers is suitable candidate for this
purpose. Especially, for its computational efficiency, it can be readily applied simulations with large ensembles and resolutions,
such as, the Coupled Model Intercomparison Project Phase 6.

Acknowledgements. This work and its contributors (LG, MED, PLV, AGT) were supported by the UKChina Research and Innovation Part-
295 nership Fund through the Met Office Climate Science for Service Partnership (CSSP) China as part of the Newton Fund. LG was also funded
by the UK National Centre for Atmospheric Science Visiting Scientist Programme. RJE acknowledges the Innovational Research Incentives
Scheme with project number 016.Veni.181.015, which is financed by the Netherlands Organisation for Scientific Research (NWO). NPK
was also funded by a UK Natural Environment Research Council Independent Research Fellowship (NE/L010976/1).



References

- 300 Berrisford, P., Dee, D., Poli, P., Brugge, R., Fielding, K., Fuentes, M., Kållberg, P., Kobayashi, S., Uppala, S., and Simmons, A.: The ERA-Interim archive Version 2.0, Shinfield Park, Reading, 2011.
- Chen, H. and Sun, J.: Assessing model performance of climate extremes in China: an intercomparison between CMIP5 and CMIP3, *Climate Change*, 129, 197–211, <https://doi.org/10.1007/s10584-014-1319-5>, 2015.
- Curio, J., Maussion, F., and Scherer, D.: A 12-year high-resolution climatology of atmospheric water transport over the Tibetan Plateau, *Earth System Dynamics*, 6, 109–124, <https://doi.org/10.5194/esd-6-109-2015>, 2015.
- 305 Dee, D. P., Uppala, S. M., Simmons, A. J., Berrisford, P., Poli, P., Kobayashi, S., Andrae, U., Balmaseda, M. A., Balsamo, G., Bauer, P., Bechtold, P., Beljaars, A. C. M., van de Berg, L., Bidlot, J., Bormann, N., Delsol, C., Dragani, R., Fuentes, M., Geer, A. J., Haimberger, L., Healy, S. B., Hersbach, H., Hólm, E. V., Isaksen, I., Kållberg, P., Köhler, M., Matricardi, M., McNally, A. P., Monge-Sanz, B. M., Morcrette, J.-J., Park, B.-K., Peubey, C., de Rosnay, P., Tavolato, C., Thèpaut, J.-N., and Vitarta, F.: The ERA-Interim reanalysis: configuration and performance of the data assimilation system, *Quarterly Journal of the Royal Meteorological Society*, 137, 553–597, <https://doi.org/10.1002/qj.828>, 2011.
- 310 Demory, M.-E., Vidale, P. L., Roberts, M. J., Berrisford, P., Strachan, J., Schiemann, R., and Mizielinski, M. S.: The role of horizontal resolution in simulating drivers of the global hydrological cycle, *Climate Dynamics*, 42, 2201–2225, <https://doi.org/10.1007/s00382-013-1924-4>, 2014.
- 315 Dong, B., Sutton, R. T., Shaffrey, L., and Klingaman, N. P.: Attribution of Forced Decadal Climate Change in Coupled and Uncoupled Ocean–Atmosphere Model Experiments, *Journal of Climate*, 30, 6203–6223, <https://doi.org/10.1175/JCLI-D-16-0578.1>, 2017.
- Donlon, C. J., Martin, M., Stark, J., Roberts-Jones, J., Fiedler, E., and Wimmer, W.: The Operational Sea Surface Temperature and Sea Ice Analysis (OSTIA) system, *Remote Sensing of Environment*, 116, 140–158, <https://doi.org/10.1016/j.rse.2010.10.017>, 2012.
- Fremme, A. and Sodemann, H.: The influence of wind and land evapotranspiration on the variability of moisture sources and precipitation of the Yangtze River Valley, *Hydrology and Earth System Sciences Discussions*, 2019, 1–31, <https://doi.org/10.5194/hess-2018-629>, 2019.
- 320 Fu, X., Bin, W., and Li, T.: Impacts of Air–Sea Coupling on the Simulation of Mean Asian Summer Monsoon in the ECHAM4 Model, *Monthly Weather Review*, 130, 2889–2904, [https://doi.org/10.1175/1520-0493\(2002\)130<2889:IOASCO>2.0.CO;2](https://doi.org/10.1175/1520-0493(2002)130<2889:IOASCO>2.0.CO;2), 2002.
- Guo, L., Klingaman, N. P., Demory, M.-E., Vidale, P. L., Turner, A. G., and Stephan, C. C.: The contributions of local and remote atmospheric moisture fluxes to East Asian precipitation and its variability, *Climate Dynamics*, Online, <https://doi.org/10.1007/s00382-017-4064-4>, 2018.
- 325 Guo, L., van der Ent, R. J., Klingaman, N. P., Demory, M.-E., Vidale, P. L., Turner, A. G., Stephan, C. C., and Chevuturi, A.: Moisture Sources for East Asian Precipitation: Mean Seasonal Cycle and Interannual Variability, *Journal of Hydrometeorology*, 20, 657–672, <https://doi.org/10.1175/JHM-D-18-0188.1>, 2019.
- Gupta, A. S., Jourdain, N. C., Brown, J. N., and Monselesan, D.: Climate Drift in the CMIP5 Models, *Journal of Climate*, 26, 8597–8615, <https://doi.org/10.1175/JCLI-D-12-00521.1>, 2013.
- 330 Hirons, L. C., Klingaman, N. P., and Woolnough, S. J.: The Impact of Air–Sea Interactions on the Representation of Tropical Precipitation Extremes, *Journal of Advances in Modeling Earth Systems*, 10, 550–559, <https://doi.org/10.1002/2017MS001252>, 2018.
- Hunke, E. C. and Lipscomb, W. H.: CICE: The Los Alamos sea ice model, documentation and software. Version 3.1, Tech. Rep. Tech. Rep., LACC-98-16, Los Alamos National Laboratory, Los Alamos, NM, 2004.



- 335 Jiang, Z., Li, W., Xu, J., and Li, L.: Extreme Precipitation Indices over China in CMIP5 Models. Part I: Model Evaluation, *Journal of Climate*, 28, 8603–8619, <https://doi.org/10.1175/JCLI-D-15-0099.1>, 2015.
- Johnson, S. J., Levine, R. C., Turner, A. G., Martin, G. M., Woolnough, S. J., Schiemann, R., Mizielinski, M. S., Roberts, M. J., Vidale, P. L., Demory, M.-E., and Strachan, J.: The resolution sensitivity of the South Asian monsoon and Indo-Pacific in a global 0.35° AGCM, *Climate Dynamics*, 46, 807–831, <https://doi.org/10.1007/s00382-015-2614-1>, 2016.
- 340 Keys, P. W., Barnes, E. A., van der Ent, R. J., and Gordon, L. J.: Variability of moisture recycling using a precipitationshed framework, *Hydrology and Earth System Sciences*, 18, 3937–3950, <https://doi.org/10.5194/hess-18-3937-2014>, 2014.
- Liepert, B. G. and Previdi, M.: Inter-model variability and biases of the global water cycle in CMIP3 coupled climate models, *Environmental Research Letters*, 7, 014006, <https://doi.org/10.1088/1748-9326/7/1/014006>, 2012.
- Lin, R., Zhou, T., and Qian, Y.: Evaluation of Global Monsoon Precipitation Changes based on Five Reanalysis Datasets, *Journal of Climate*, 27, 1271–1289, <https://doi.org/10.1175/JCLI-D-13-00215.1>, 2014.
- 345 Madec, G.: NEMO ocean engine, Tech. Rep. Tech. Rep. 27, Note du Pole de modélisation, Institut Pierre-Simon Laplace (IPSL), 2008.
- Marathayil, D., Turner, A. G., Shaffrey, L. C., and Levine, R. C.: Systematic winter sea-surface temperature biases in the northern Arabian Sea in HiGEM and the CMIP3 models, *Environmental Research Letters*, 8, 1–6, <https://doi.org/10.1088/1748-9326/8/1/014028>, 2013.
- Ogata, T., Johnson, S. J., Schiemann, R., Demory, M., Mizuta, R., Yoshida, K., and Arakawa, O.: The resolution sensitivity of the Asian summer monsoon and its inter-model comparison between MRI-AGCM and MetUM, *Climate Dynamics*, 49, 3345–3361, <https://doi.org/10.1007/s00382-016-3517-5>, 2017.
- 350 Ou, T., Chen, D., Linderholm, H. W., and Jeong, J.-H.: Evaluation of global climate models in simulating extreme precipitation in China, *Tellus A: Dynamic Meteorology and Oceanography*, 65, 19799, <https://doi.org/10.3402/tellusa.v65i0.19799>, 2013.
- Ratnam, J. V., Morioka, Y., Behera, S. K., and Yamagata, T.: A model study of regional air-sea interaction in the austral summer precipitation over southern Africa, *Journal of Geophysical Research: Atmospheres*, 120, 2342–2357, <https://doi.org/10.1002/2014JD022154>, 2015.
- 355 Rodríguez, J. M., Milton, S. F., and Marzin, C.: The East Asian Atmospheric Water Cycle and Monsoon Circulation in the Met Office Unified Model, *Journal of Geophysical Research: Atmospheres*, 122, 10,246–10,265, <https://doi.org/10.1002/2016JD025460>, 2017.
- Schanze, J. J., Schmitt, R. W., and Yu, L. L.: The global oceanic freshwater cycle: A state-of-the-art quantification, *Journal of Marine Research*, 68, 569–595, <https://doi.org/10.1357/002224010794657164>, 2010.
- 360 Schiemann, R., Demory, M.-E., Mizielinski, M. S., Roberts, M. J., Shaffrey, L. C., Strachan, J., and Vidale, P. L.: The sensitivity of the tropical circulation and Maritime Continent precipitation to climate model resolution, *Climate Dynamics*, 42, 2455–2468, <https://doi.org/10.1007/s00382-013-1997-0>, 2014.
- Sperber, K. R., Annamalai, H., Kang, I.-S., A.Kitoh, A.Moise, A.Turner, B.Wang, and Zhou, T.: The Asian summer monsoon: an intercomparison of CMIP5 vs. CMIP3 simulations of the late 20th century, *Climate Dynamics*, 41, 2711–2744, <https://doi.org/10.1007/s00382-012-1607-6>, 2013.
- 365 Stephan, C. C., Klingaman, N. P., Vidale, P. L., Turner, A. G., Demory, M.-E., and Guo, L.: A Comprehensive Analysis of Coherent Rainfall Patterns in China and Potential Drivers. Part I: Interannual Variability, *Climate Dynamics*, Published online, <https://doi.org/10.1007/s00382-017-3882-8>, 2018a.
- Stephan, C. C., Klingaman, N. P., Vidale, P. L., Turner, A. G., Demory, M.-E., and Guo, L.: Interannual rainfall variability over China in the MetUM GA6 and GC2 configurations, *Geoscientific Model Development*, 11, 1823–1847, <https://doi.org/10.5194/gmd-11-1823-2018>, 2018b.
- 370



- Su, T., Feng, T., and Feng, G.: Evaporation variability under climate warming in five reanalyses and its association with pan evaporation over China, *Journal of Geophysical Research*, 120, 8080–8098, <https://doi.org/10.1002/2014JD023040>, 2015.
- Terai, C. R., Caldwell, P. M., Klein, S. A., Tang, Q., and Branstetter, M. L.: The atmospheric hydrologic cycle in the ACME v0.3 model, *Climate Dynamics*, 50, 3251–3279, <https://doi.org/10.1007/s00382-017-3803-x>, 2018.
- 375 Valcke, S.: The OASIS3 coupler: a European climate modelling community software, *Geoscientific Model Development*, 6, 373–388, <https://doi.org/10.5194/gmd-6-373-2013>, 2013.
- van der Ent, R. J., Turinenburg, O. A., Knoche, H.-R., Kunstmann, H., and Savenije, H. H.: Should we use a simple or complex model for moisture recycling and atmospheric moisture tracking?, *Hydrology and Earth System Sciences*, 17, 4869–4884, <https://doi.org/10.5194/hess-17-4869-2013>, 2013.
- 380 van der Ent, R. J., Wang-Erlandsson, L., Keys, P. W., and Savenije, H. H. G.: Contrasting roles of interception and transpiration in the hydrological cycle – Part 2: Moisture recycling, *Earth System Dynamics*, 5, 471–489, <https://doi.org/10.5194/esd-5-471-2014>, 2014.
- van Haren, R., Haarsma, R. J., Van Oldenborgh, G. J., and Hazeleger, W.: Resolution Dependence of European Precipitation in a State-of-the-Art Atmospheric General Circulation Model, *Journal of Climate*, 28, 5134–5149, <https://doi.org/10.1175/JCLI-D-14-00279.1>, 2015.
- 385 Vanni re, B., Demory, M.-E., Vidale, P. L., Schiemann, R., Roberts, M. J., Roberts, C. D., Matsueda, M., Terray, L., Koenigk, T., and Senan, R.: Multi-model evaluation of the sensitivity of the global energy budget and hydrological cycle to resolution, *Climate Dynamics*, 52, 6817–6846, <https://doi.org/10.1007/s00382-018-4547-y>, 2018.
- Vellinga, M., Roberts, M., Vidale, P. L., Mizielinski, M. S., Demory, M.-E., Schiemann, R., Strachan, J., and Bain1, C.: Sahel decadal rainfall variability and the role of model horizontal resolution, *Geophysical Research Letters*, 43, 326–333, <https://doi.org/10.1002/2015GL066690>, 2016.
- 390 Walters, D., Boutle, I., Brooks, M., Melvin, T., Stratton, R., Vosper, S., Wells, H., Williams, K., Wood, N., Allen, T., Bushell, A., Copsey, D., Earnshaw, P., Edwards, J., Gross, M., Hardiman, S., Harris, C., Heming, J., Klingaman, N., Levine, R., Manners, J., Martin, G., Milton, S., Mittermaier, M., Morcrette, C., Riddick, T., Roberts, M., Sanchez, C., Selwood, P., Stirling, A., Smith, C., Suri, D., Tennant, W., Vidale, P. L., Wilkinson, J., Willett, M., Woolnough, S., and Xavier, P.: The Met Office Unified Model Global Atmosphere 6.0/6.1 and JULES
- 395 Global Land 6.0/6.1 configurations, *Geoscientific Model Development*, 10, 1487–1520, <https://doi.org/10.5194/gmd-10-1487-2017>, 2017.
- Wang, H. and Chen, H.: Climate control for southeastern China moisture and precipitation: Indian or East Asian monsoon?, *Journal of Geophysical Research*, 117, <https://doi.org/10.1029/2012JD017734>, 2012.
- Wei, J., Dirmeyer, P. A., Bosilovich, M. G., and Wu, R.: Water vapor sources for Yangtze River Valley rainfall: Climatology, variability, and implications for rainfall forecasting, *Journal of Geophysical Research*, 117, D05 126, <https://doi.org/10.1029/2011JD016902>, 2012.
- 400 Wen, X., Fang, G., Qi, H., Zhou, L., and Gao, Y.: Changes of temperature and precipitation extremes in China: past and future, *Theoretical and Applied Climatology*, 126, 369–383, <https://doi.org/10.1007/s00704-015-1584-x>, 2016.
- Williams, K. D., Harris, C. M., Bodas-Salcedo, A., Camp, J., Comer, R. E., Copsey, D., Fereday, D., Graham, T., Hill, R., Hinton, T., Hyder, P., Ineson, S., Masato, G., Milton, S. F., Roberts, M. J., Rowell, D. P., Sanchez, C., Shelly, A., Sinha, B., Walters, D. N., West, A., Woollings, T., and Xavier, P. K.: The Met Office Global Coupled model 2.0 (GC2) configuration, *Geoscientific Model Development*, 8, 1509–1524, <https://doi.org/10.5194/gmd-8-1509-2015>, 2015.
- 405 Yang, B., Zhang, Y., Qian, Y., Song, F., Leung, L. R., Wu, P., Guo, Z., Lu, Y., and Huang, A.: Better monsoon precipitation in coupled climate models due to bias compensation, *npj Climate and Atmospheric Science*, 2, <https://doi.org/10.1038/s41612-019-0100-x>, 2019.
- Yang, S., Feng, J., Dong, W., and Chou, J.: Analyses of extreme climate events over china based on CMIP5 historical and future simulations, *Advances in Atmospheric Sciences*, 31, 1209–1220, <https://doi.org/10.1007/s00376-014-3119-2>, 2014.



- 410 Yatagai, A., Kamiguchi, K., Arakawa, O., Hamada, A., Yasutomi, N., and Kitoh, A.: APHRODITE: Constructing a Long-Term Daily Gridded Precipitation Dataset for Asia Based on a Dense Network of Rain Gauges, *Bulletin of the American Meteorological Society*, 93, 1401–1415, <https://doi.org/10.1175/BAMS-D-11-00122.1>, 2012.
- Zhang, C., Tang, Q., and Chen, D.: Recent changes in the moisture source of precipitation over the Tibetan Plateau, *Journal of Climate*, 30, 1807–1819, <https://doi.org/10.1175/JCLI-D-15-0842.1>, 2017.
- 415 Zhou, T.-J. and Yu, R.-C.: Atmospheric water vapor transport associated with typical anomalous summer rainfall patterns in China, *Journal of Geophysical Research*, 110, D08 104, <https://doi.org/10.1029/2004JD005413>, 2005.

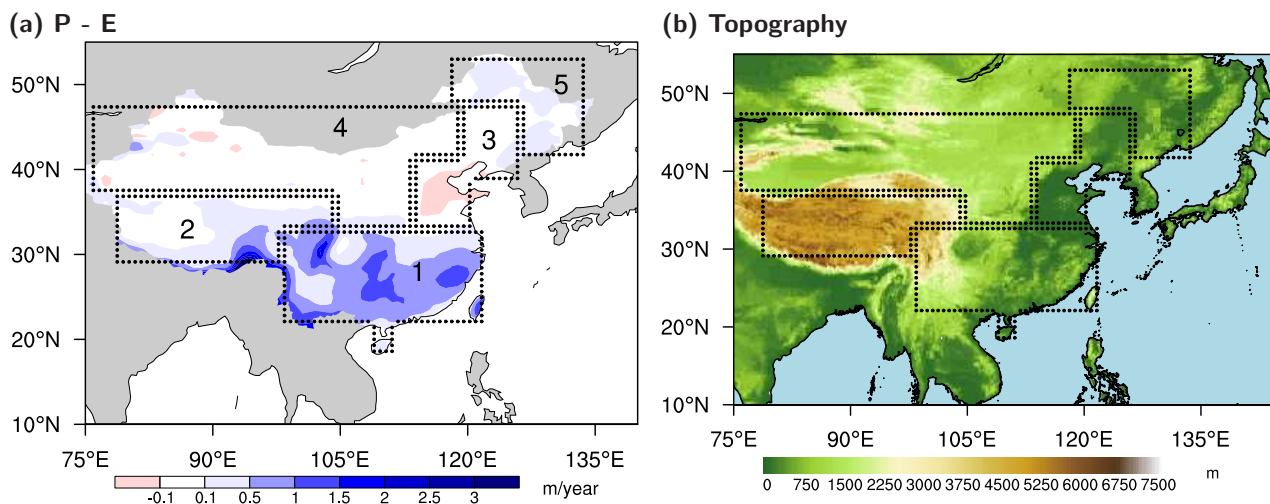


Figure 1. (a) Annual mean precipitation minus evaporation ($P - E$), calculated using the ERA-Interim reanalysis during 1979–2016, units: m/year; (b) Topography over the EA landmass, units: m. Boxes 1–5 in (a) indicate subregions over EA. This is reproduced from Guo et al. (2018).

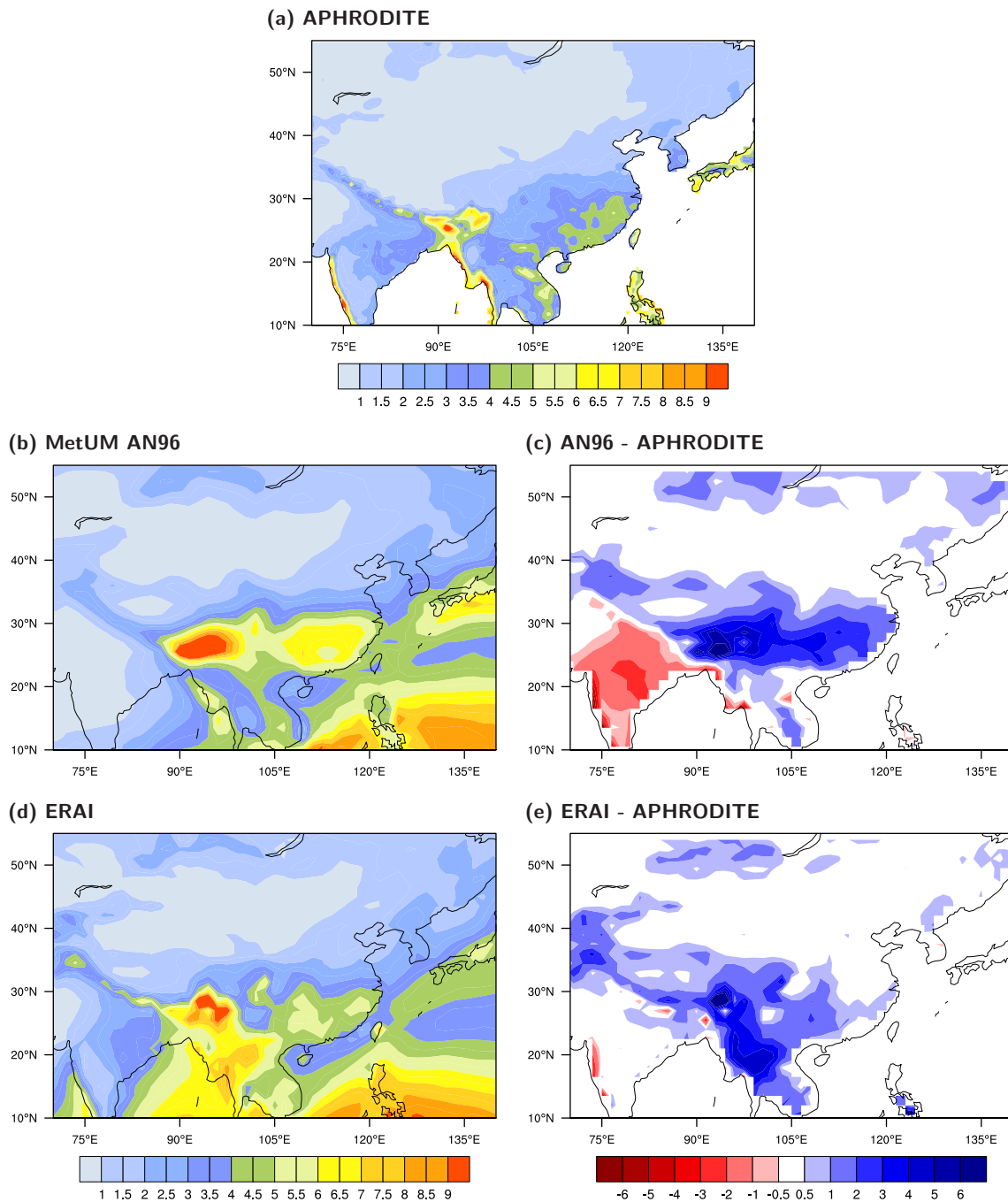


Figure 2. Annual mean precipitation from (a) APHRODITE, (b) MetUM AN96 and (d) ERA-Interim, and differences (c) between AN96 and APHRODITE and (e) between ERA-Interim and APHRODITE. Units: $\text{mm} \cdot \text{day}^{-1}$.

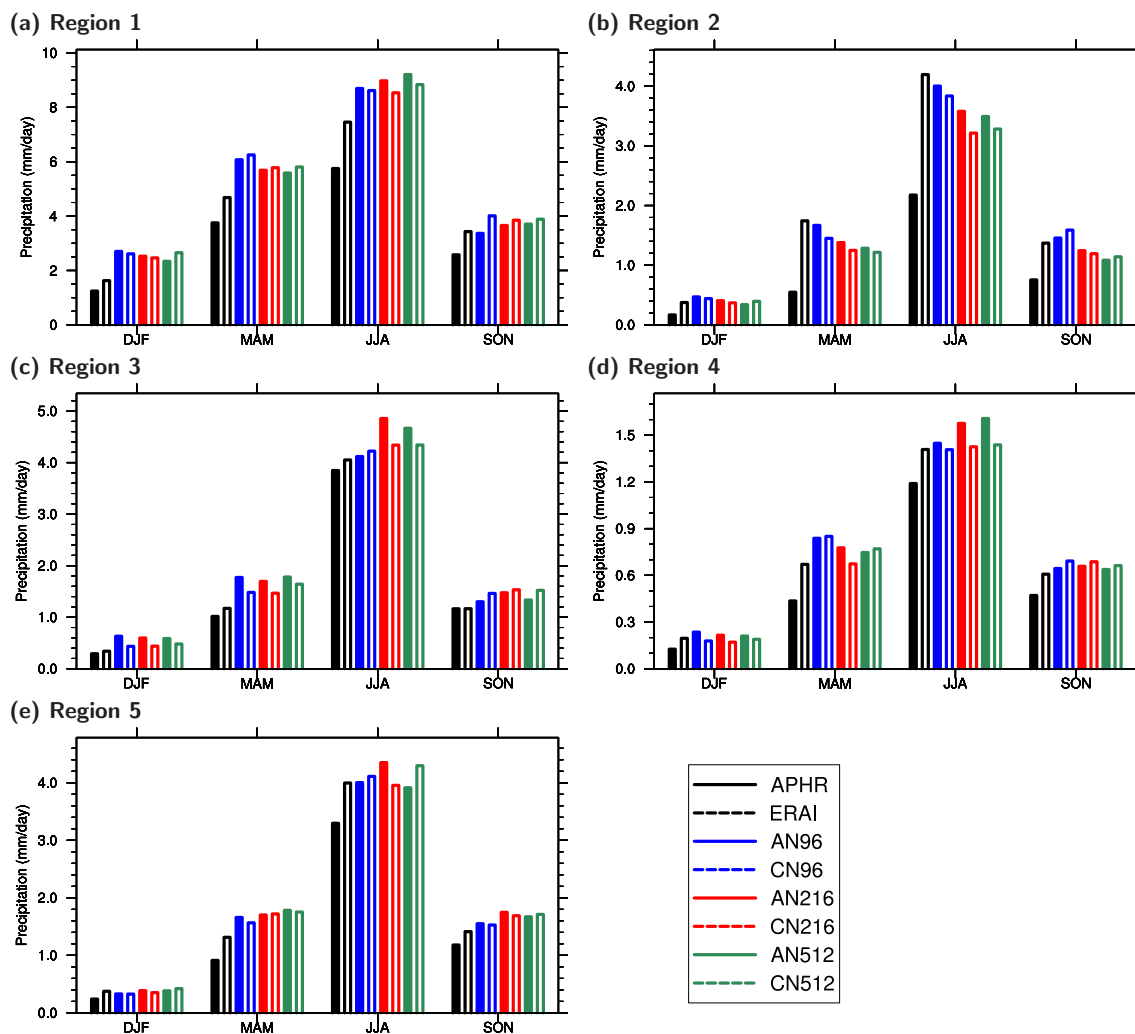


Figure 3. Seasonal and regional mean precipitation over EA subregions. Compared datasets include APHRODITE, ERA-Interim, AN96, CN96, AN216, CN216, AN512 and CN512. Units: $\text{mm} \cdot \text{day}^{-1}$.

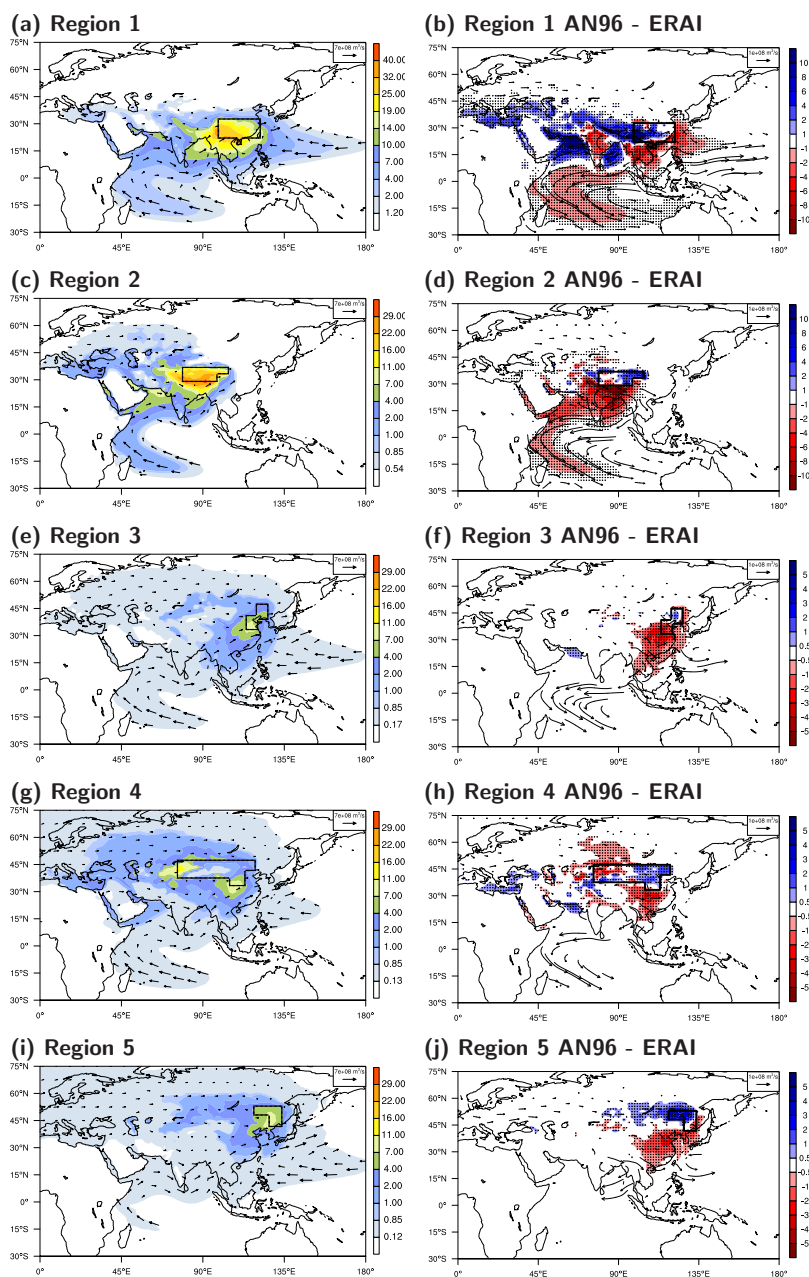
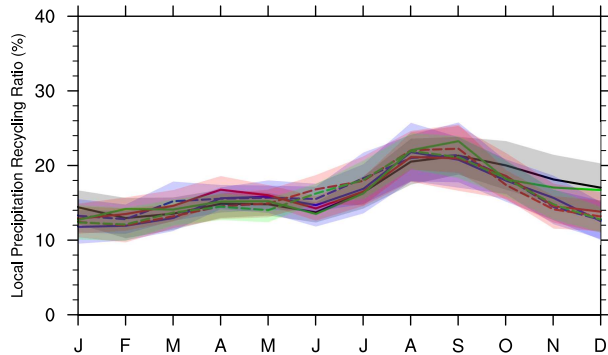


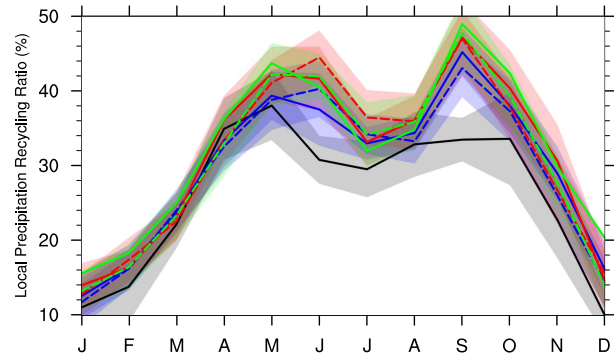
Figure 4. Annual mean moisture source for EA subregions (a, c, e, g and i, units: $\text{mm} \cdot \text{month}^{-1}$) and vertically integrated moisture flux (vector, units: $\text{m}^3 \cdot \text{s}^{-1}$) calculated from ERA-Interim. The moisture source region that accounts for 80% of precipitation is shown. Difference in annual mean moisture sources between AN96 and ERA-Interim (b, d, f, h and j). Units: $\text{mm} \cdot \text{month}^{-1}$. Differences that are significant at the 1% level are hatched. The black box in each panel indicates the target region.



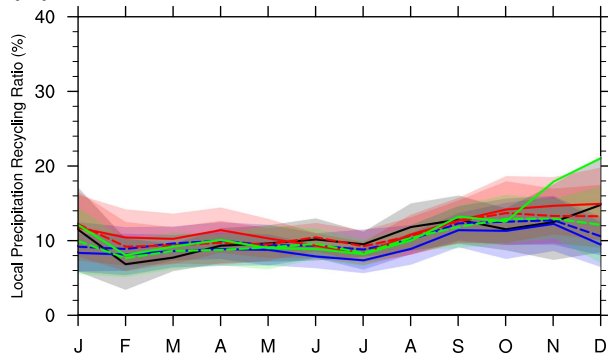
(a) Region 1



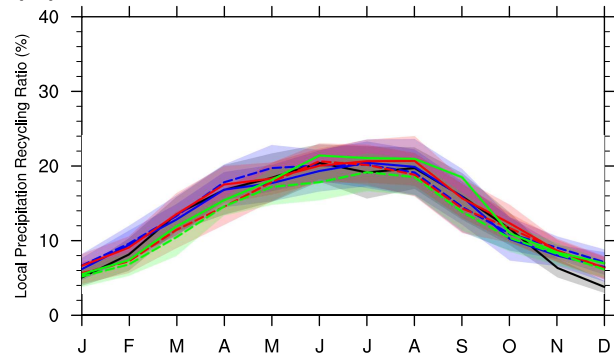
(b) Region 2



(c) Region 3



(d) Region 4



(e) Region 5

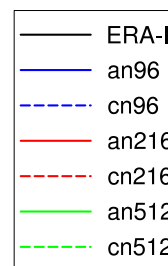
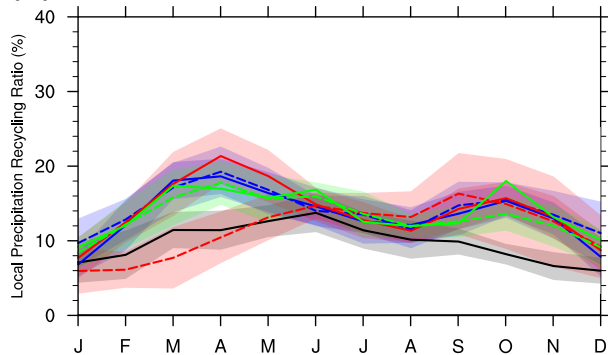


Figure 5. Annual cycle of precipitation recycling ratio for EA subregions, units: %.

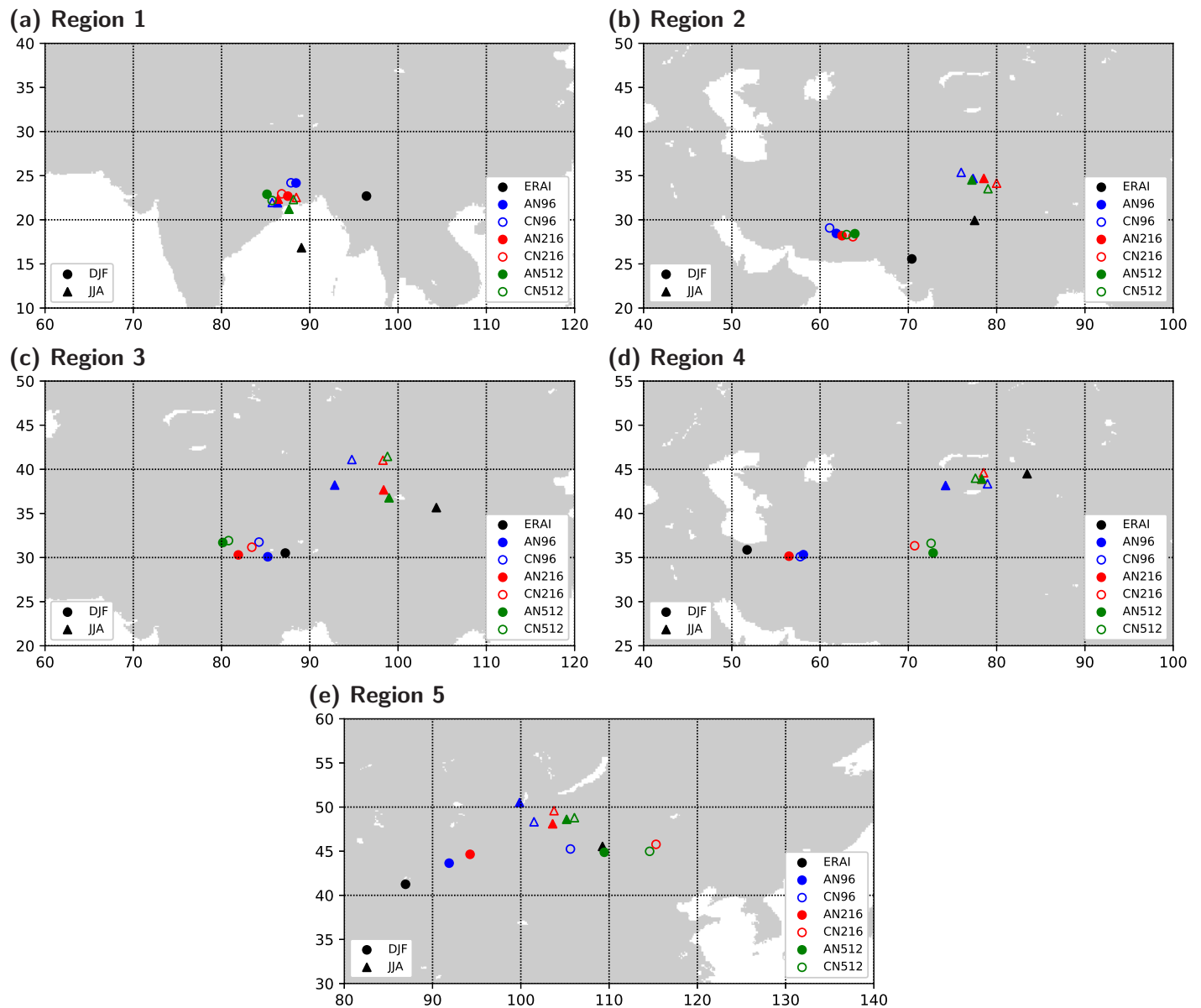


Figure 6. Mass centres of moisture source in DJF and JJA for regions 1-5 from ERA-Interim and MetUM simulations.

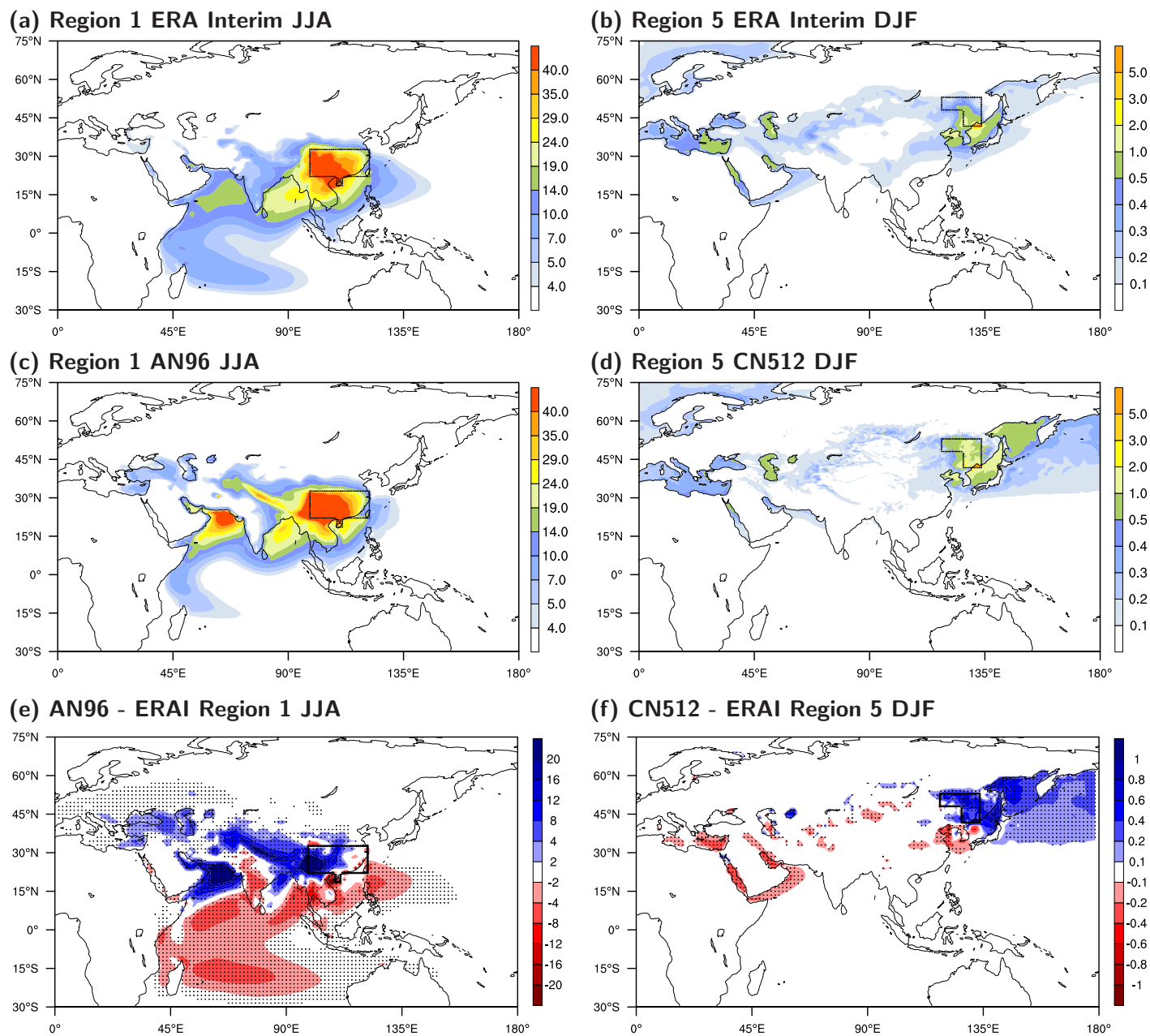


Figure 7. Moisture sources during JJA for region 1 from ERA-Interim (a) and AN96 (c). Moisture sources during DJF for region 5 from ERA-Interim (b) and CN512 (d). Difference of moisture sources in region 1 JJA (e) between AN96 and ERA-Interim (f) between CN512 and ERA-Interim. Units: $\text{mm} \cdot \text{month}^{-1}$. The black box in each panel represents the target regions. Details of the division can be found in Figure 1. Differences that are significant at the 1% level are hatched.

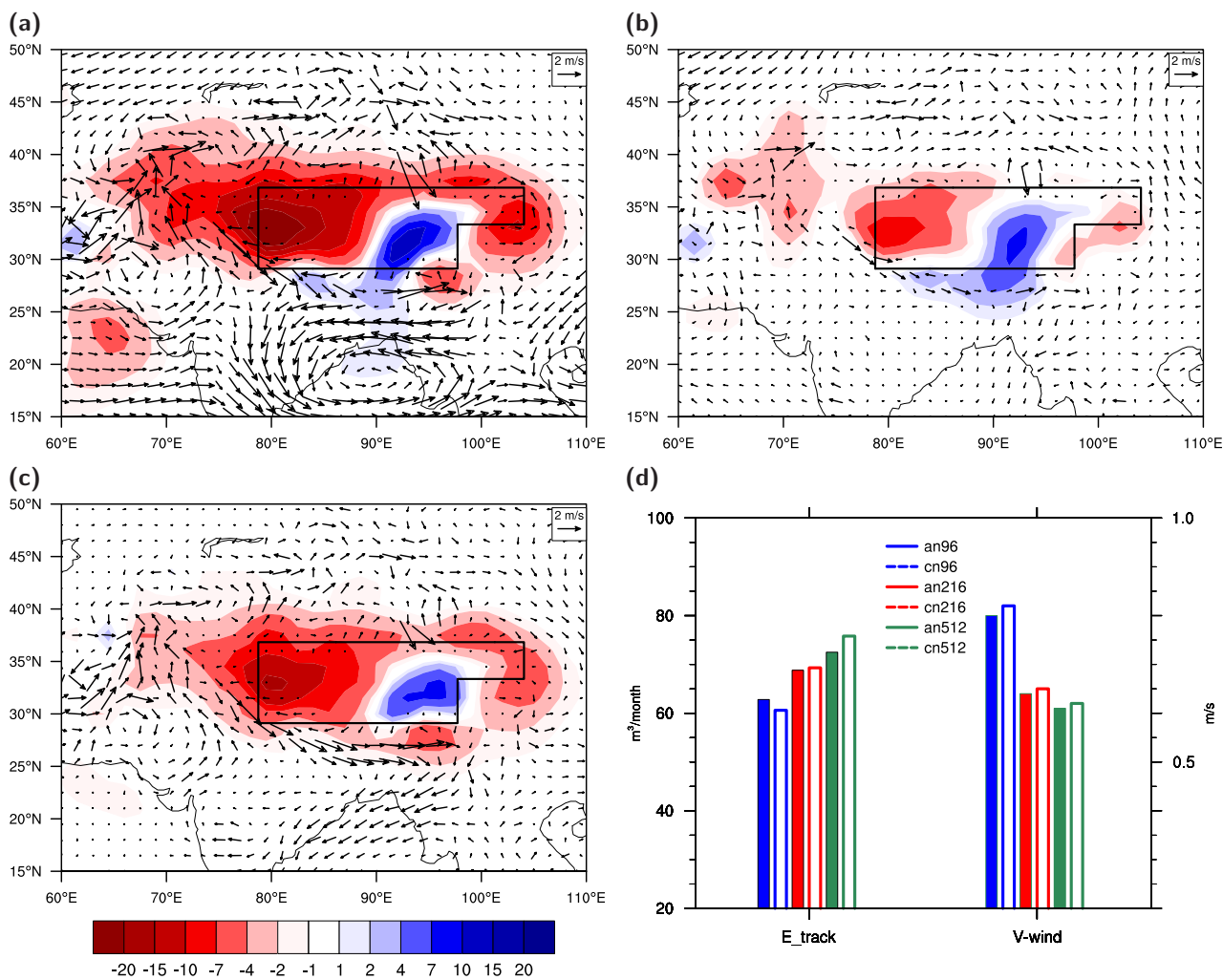


Figure 8. Differences of tracked evaporation (colour, units: $\text{mm} \cdot \text{month}^{-1}$) and 700 hPa wind (vector, units: $\text{m} \cdot \text{s}^{-1}$) in JJA over Tibetan Plateau (region 2) between (a) CN512-AN96, (b) CN512-CN216 and (c) CN216-CN96. (d) Seasonal mean tracked evaporation (E_{track} , $\text{m}^3 \cdot \text{month}^{-1}$) over eastern Tibet and the 700 hPa meridional wind (V_{wind} , $\text{m} \cdot \text{s}^{-1}$) along the southern boundary of the eastern Tibetan Plateau.

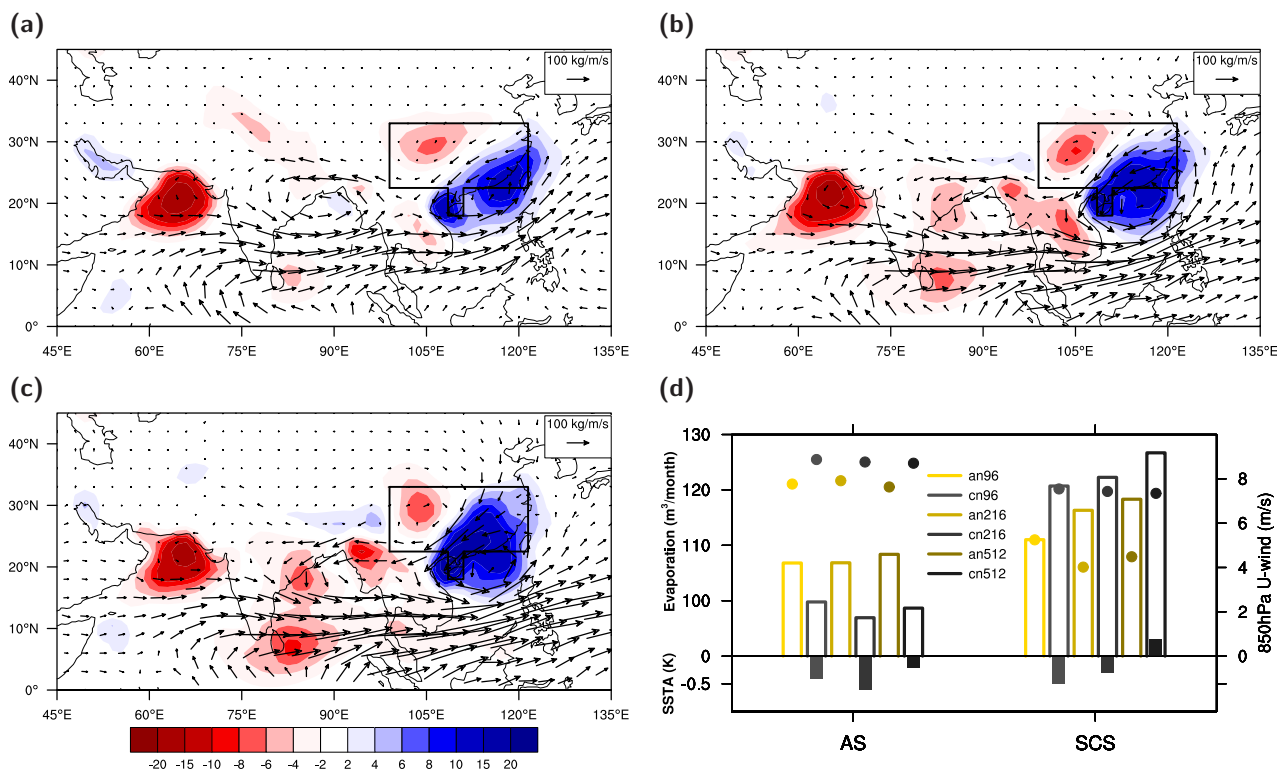


Figure 9. Differences in moisture sources for precipitation over region 1 JJA between air-sea coupled and atmosphere-only simulations: (a) CN96 minus AN96, (b) CN216 minus AN216 and (c) CN512 minus AN512. Units: $\text{mm} \cdot \text{month}^{-1}$. Vectors are differences in the vertically integrated moisture flux, units: $\text{kg} \cdot \text{m}^{-1} \cdot \text{s}^{-1}$. (d) Mean evaporation (bars with outline-only, $\text{m}^3 \cdot \text{month}^{-1}$), mean zonal wind (dot, $\text{m} \cdot \text{s}^{-1}$) and sea surface temperature anomaly from ERA-Interim and OSTIA (filled bar, units: K) over the Arabian Sea (AS) and South China Sea (SCS).

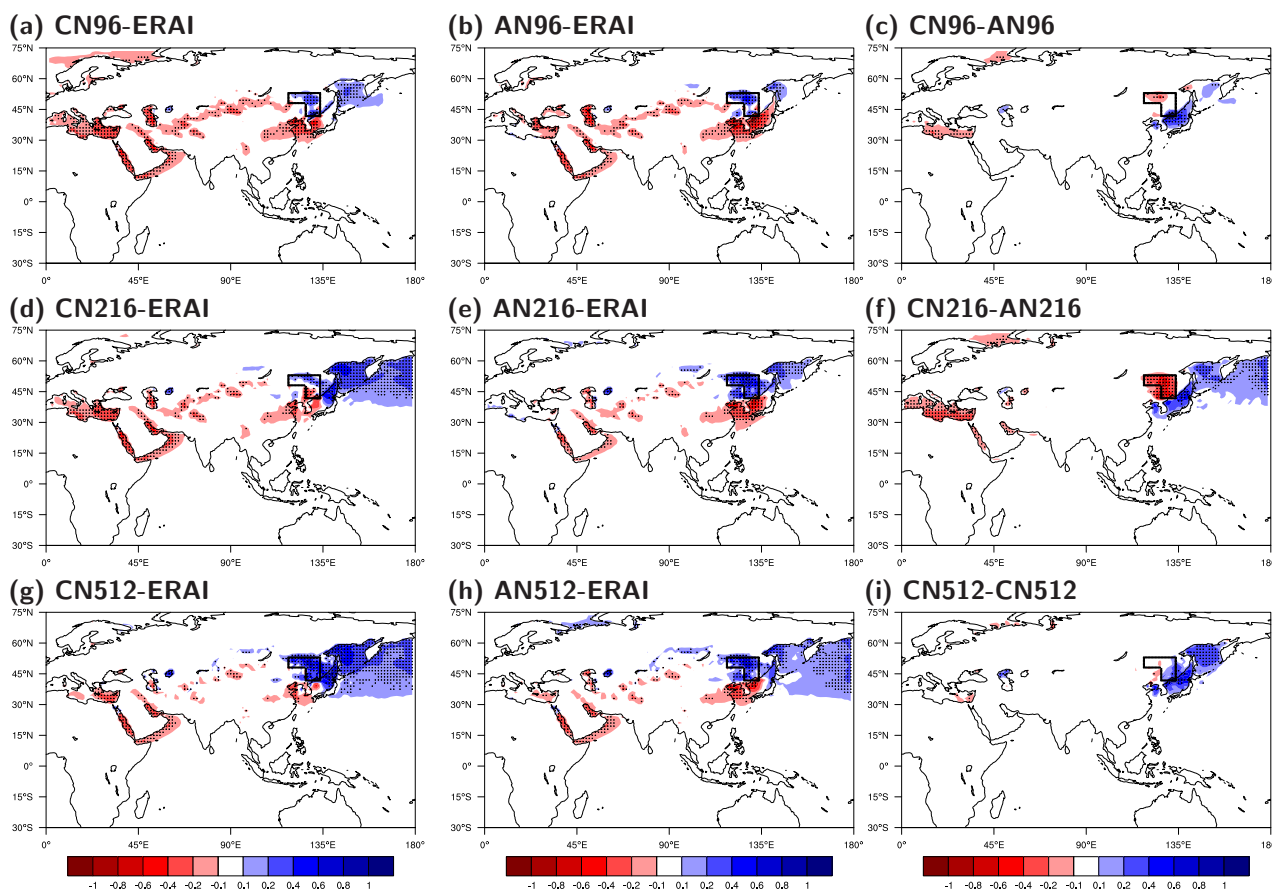


Figure 10. Differences in moisture sources for region 5 in DJF. Units: mm/month.

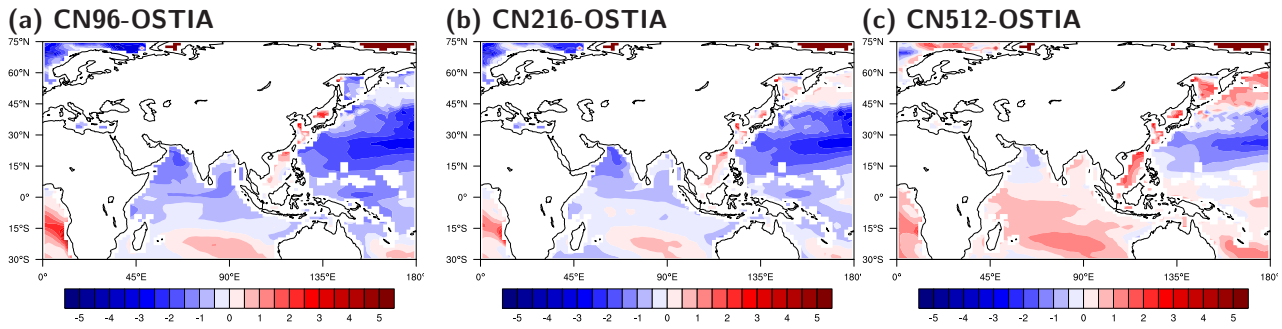


Figure 11. SST bias in MetUM coupled simulation in DJF against OSTIA. Units: K.



Table 1. Simulations used in this study.

Simulation	Atmosphere		Ocean		Period
	horizontal	vertical	horizontal	vertical	
AN96	1.875×1.25	L85	-	-	1982-2012
CN96	1.875×1.25	L85	0.25	L75	31yr present day
AN216	0.56×0.83	L85	-	-	1982-2012
CN216	0.56×0.83	L85	0.25	L75	31yr present day
AN512	0.35×0.23	L85	-	-	1992-2012
CN512	0.35×0.23	L85	0.25	L75	21yr present day



Table 2. Root-mean-square deviation of monthly precipitation recycling ratio (%) measured between MetUM simulations and ERA-Interim over five EA subregions.

	AN96	CN96	AN216	CN216	AN512	CN512
cn1	1.8	1.8	1.7	2.0	2.0	1.9
cn2	5.2	4.8	6.4	6.6	4.9	6.3
cn3	1.7	1.6	1.8	1.3	1.5	1.3
cn4	1.4	1.6	1.3	1.5	1.8	1.7
cn5	4.6	5.0	5.3	3.3	2.8	4.0



Table 3. Annual and seasonal mean contributions to regional precipitation (regions 1-5, units: %) from the tropical ocean (T_s), tropical land (T_l), extratropical ocean (X_s), extratropical land (X_l) and local precipitation recycling (ρ). The solstices latitudes (23.4°N and 23.4°S) are used to separate the tropics and the extra-tropics. In each column, seven values represent seven datasets, shown in the order as the ERA-Interim, AN96, CN96, AN216, CN216, AN512 and CN512. Values with boldface highlight difference that is discussed in Section 4.3.

Region	Season	T_s					T_l					X_s					X_l					ρ														
		ET	A9	C9	A2	C2	A5	C5	ET	A9	C9	A2	C2	A5	C5	ET	A9	C9	A2	C2	A5	C5	ET	A9	C9	A2	C2	A5	C5							
1	Ann	49	35	35	39	37	39	40	11	18	19	14	13	11	12	9	5	5	8	10	12	11	15	25	25	23	23	21	21	16	16	17	16	17	17	16
	DJF	40	37	36	41	39	42	39	15	21	22	15	15	12	11	15	8	6	12	15	17	19	17	23	23	20	19	17	18	14	12	13	13	12	12	12
	MAM	43	36	34	39	38	41	40	15	20	22	15	14	12	13	7	4	3	6	9	11	10	20	25	26	24	24	22	22	14	15	15	16	14	14	15
	JJA	55	36	36	39	37	39	41	10	17	17	14	12	11	13	6	4	4	6	7	8	8	12	26	26	24	25	24	22	17	17	18	17	19	19	16
	SON	47	31	33	37	35	36	36	8	16	18	13	13	11	12	13	9	9	11	13	15	14	12	26	22	21	21	19	20	20	19	18	18	18	18	19
2	Ann	25	9	9	9	10	10	10	6	5	6	4	4	3	3	7	4	4	8	10	13	12	30	48	47	44	40	38	40	31	34	34	36	37	36	35
	DJF	27	22	22	24	22	23	22	10	12	14	8	7	4	5	17	9	9	18	25	32	31	34	42	41	35	32	27	26	12	15	14	15	15	14	16
	MAM	17	11	9	11	13	13	13	6	7	8	5	5	4	4	8	4	4	7	12	16	15	34	44	45	40	35	32	32	34	34	34	36	35	35	36
	JJA	28	6	6	6	6	7	7	6	3	4	2	2	2	2	6	3	3	5	6	8	8	30	53	52	50	47	47	48	31	35	35	36	38	37	35
	SON	28	10	10	11	11	11	10	8	5	7	4	5	4	3	7	5	5	9	11	14	13	26	39	40	34	33	29	31	32	41	39	43	41	42	43
3	Ann	28	18	14	19	16	16	20	7	10	8	7	6	4	7	12	7	7	10	13	16	14	43	57	61	53	55	55	51	10	9	10	10	10	10	9
	DJF	19	21	18	20	18	17	15	10	14	15	9	9	5	5	30	11	12	20	28	36	34	31	45	46	40	34	33	37	10	8	9	11	11	9	9
	MAM	21	17	12	16	13	13	17	9	11	9	8	5	4	5	9	5	5	8	13	16	14	52	58	64	58	59	59	56	9	9	10	10	9	9	8
	JJA	33	20	16	22	19	18	24	6	9	7	8	5	4	7	9	6	7	8	9	11	9	42	57	61	53	57	58	51	10	8	9	9	10	9	8
	SON	22	13	10	14	13	13	15	5	7	8	6	6	4	5	20	12	10	16	20	24	22	41	57	60	51	49	47	47	12	11	12	13	13	12	11
4	Ann	15	9	8	8	8	8	9	4	6	6	4	3	2	3	11	6	6	10	14	17	16	54	63	64	61	58	57	55	17	17	17	17	16	15	16
	DJF	15	11	11	11	11	10	10	6	9	10	6	4	2	3	33	14	13	25	38	46	45	39	58	58	51	40	35	37	6	8	8	8	7	6	6
	MAM	11	9	6	8	10	9	11	5	7	7	5	3	3	3	10	5	5	9	16	19	18	58	63	64	62	56	54	54	17	16	18	17	16	15	14
	JJA	16	8	7	8	7	6	9	4	4	4	3	2	2	3	6	4	4	6	8	9	10	55	64	65	62	63	64	59	20	20	20	20	20	19	20
	SON	15	10	10	9	10	9	9	5	7	8	4	4	4	3	17	9	8	15	18	22	23	50	62	62	59	56	53	52	13	12	12	13	12	12	13
5	Ann	14	7	6	7	7	7	8	3	3	3	2	2	2	2	15	8	8	11	14	16	16	58	69	70	65	65	62	61	11	14	14	14	13	14	13
	DJF	8	5	4	5	4	4	4	3	4	4	3	2	1	1	49	28	32	39	54	56	54	34	54	49	44	34	28	31	7	9	11	10	6	10	9
	MAM	9	3	3	3	5	5	5	3	2	3	2	2	1	2	14	6	6	8	14	16	15	62	71	71	67	68	62	63	12	17	17	19	11	16	15
	JJA	18	8	7	10	8	9	10	3	3	3	3	2	2	3	9	6	6	7	7	9	9	59	70	72	67	69	67	66	11	13	13	13	13	14	12
	SON	10	5	5	5	5	5	8	2	2	2	2	2	1	2	25	13	11	16	20	25	26	54	66	67	62	58	55	53	9	14	14	14	14	13	12